https://doi.org/10.5194/egusphere-2024-3087
Preprint. Discussion started: 5 November 2024

Representing improved tropospheric ozone distribution by including lightning NOx emissions in CHIMERE

Sanhita Ghosh[1], Arineh Cholakian[1], Sylvain Mailler[1, 2], and Laurent Menut[1]

[1]Laboratoire de Météorologie Dynamique, IPSL, École Polytechnique, Route de Saclay, Palaiseau, France, 91128
[2]École des Ponts, Marne-la-Vallée, Institut Polytechnique de Paris

Correspondence: Sanhita Ghosh (ghosh.sanhita@lmd.ipsl.fr; sanhitaghosh027@gmail.com)

Abstract. Estimating nitrogen oxide emissions from lightning (LNOx) in models is highly uncertain, affecting the accuracy of atmospheric composition and air quality assessments. Still, it is essential to include the emissions in model to increase the realism in representing the model outcomes. LNOx emissions have recently been incorporated into the updated version of the CHIMERE model (v2023r2). In the present study, we evaluate the present state of modelling the lightning flashes and the LNOx emissions, using a classical scheme based on cloud top height (CTH) and the model CHIMERE. We asses the impact of LNOx on tropospheric ozone (O_3) concentration over the northern hemisphere (NH) through a detailed evaluation of simulated tropospheric O_3. The total NO emission from lightning is estimated as 8.82 Tg N yr^{-1} over the NH. There is an overall increase in O_3 concentration due to inclusion of LNOx. The increase is highest in the mid to upper troposphere, specifically over the tropics. The comparison of the simulated O_3 to measurements shows that the inclusion of LNOx emissions substantially improves the tropospheric O_3 distribution, reducing bias significantly. This is particularly true for the free troposphere over the tropical region. The LNOx emissions hence critically influence the O_3 concentration as well as the concentration of hydroxyl radicals (OH). There are 15% and 40% increases, respectively, in O_3 and OH burden as observed due to the inclusion of LNOx in model, which further impact the atmospheric lifetime of trace gas methane (CH_4) by reducing it by 24%.

1 Introduction

Nitrogen oxides (NOx), consisting of nitric oxide (NO) and nitrogen dioxide (NO_2), are critical trace gases that play a key role in atmospheric chemistry, particularly in the formation of tropospheric ozone (O_3) (Finney et al., 2014; Luo et al., 2017; Akimoto and Tanimoto, 2022). NOx emissions arise from both anthropogenic sources (e.g., fossil fuel combustion, biomass burning) and natural processes, such as lightning (Verma et al., 2021; Butler et al., 2020). Among these sources, lightning-induced NOx (LNOx) contributes approximately 10%–15% to global NOx emissions, with an even greater contribution (up to 70%) in the upper troposphere (Maseko et al., 2021; Luhar et al., 2021; Wu et al., 2023). Importantly, LNOx has a stronger impact on tropospheric O_3 formation compared to surface-based sources, due to the altitude at which LNOx is injected into the atmosphere and the efficiency of O_3 production in the upper troposphere (Finney et al., 2016a; Luhar et al., 2021). However, the estimated rate of NOx emissions due to lightning is highly uncertain, ranging from 8 mol NO to 4000 mol NO per flash

https://doi.org/10.5194/egusphere-2024-3087
Preprint. Discussion started: 5 November 2024

(Finney et al., 2016a; Arndt et al., 2019), although Schumann and Huntrieser (2007) suggest a value of 250 mol NO per flash. Nevertheless, inclusion of these emissions in models is essential to enhance the accuracy and reliability of model projections.

The inclusion of LNOx in chemistry-transport models has been the focus of research for several decades (Kang et al., 2020), with seminal studies by Price and Rind (1992); Price et al. (1997a); Schumann and Huntrieser (2007); Allen et al. (2010); Finney et al. (2014), pioneering the quantification of lightning flash rates and their associated NOx production. These foundational studies laid the groundwork for understanding the contribution of LNOx to tropospheric chemistry (Allen et al., 2010; Banerjee et al., 2014; Finney et al., 2016a; Kang et al., 2019, 2020). A range of parameterization schemes, including diverse empirical equations, have been developed over decades to quantify lightning flash rates and their spatial distribution (Finney et al., 2014). Despite the significant progress made, challenges remain in accurately quantifying LNOx emissions, due to uncertainties in characterizing both the spatial and temporal variations in lightning frequency and intensity, the apportionment among 'cloud to ground (CG)' and 'in cloud (IC)' flashes, the rates of NOx production from lightning discharges, as well as the vertical distribution and transportation of LNOx after its generation (Labrador et al., 2005; Schumann and Huntrieser, 2007; Menut et al., 2020a; Wu et al., 2023). Recent studies have focused on improving the representation of lightning in models through various parameterization schemes, including cloud top height (CTH) (Price and Rind, 1992; Price et al., 1997c; Clark et al., 2017), ice flux (Finney et al., 2014), convective precipitation, updraught of mass flux (Allen et al., 2000; Allen and Pickering, 2002) and convective available potential energy (CAPE) (Choi et al., 2005; Zhao et al., 2009). These approaches aim to better capture the spatial and temporal variability of lightning activity, leading to more accurate estimates of LNOx emissions.

In this study, we expand upon the previous work by utilizing the most frequently used CTH scheme in the CHIMERE chemistry-transport model to evaluate the current state of LNOx modelling. The model CHIMERE was developed in 1997 and has been modified on a regular basis for better prediction of atmospheric substances (Menut et al., 2020b). The improvement in the natural emissions in the recent version of the model allows the incorporation of LNOx emissions (Menut et al., 2024). The study by Menut et al. (2020a), conducted over a short period of two months (July–August, 2013), demonstrates changes in tropospheric O_3 and NOx concentrations resulting from the inclusion of LNOx emissions in CHIMERE. However, opportunities remain to improve the representation of flash rates by applying correction factors. A comprehensive evaluation of simulated tropospheric O_3 is also essential to refine model accuracy and deepen our understanding in the role of LNOx in regional air quality and atmospheric composition.

Furthermore, lightning-generated NOx also influences the tropospheric hydroxyl radical (OH) budget, in addition to affecting O_3 concentrations (Murray et al., 2013; Murray, 2016). The OH radical is primarily formed due to photolysis of O_3 ($O(^1D)$) at a shorter wavelength ($\leq$330 nm) in the presence of water vapour and secondarily through the reaction between hydroperoxyl radical (HO_2) and NO (Lelieveld et al., 2016; Banerjee et al., 2014). As a highly reactive and short-lived oxidant, with a lifetime of just a few seconds, OH is essential to tropospheric chemistry (Lelieveld et al., 2016). However, significant variability exists among global models, which differ by as much as ($\pm$30%) in estimating the mean OH burden (Murray et al., 2021). OH further controls the lifetime of many important trace gases, such as methane (CH_4), carbon monoxide (CO) and non-methane VOCs (NMVOCs) (Akimoto and Tanimoto, 2022; Luhar et al., 2021). For example, increase in OH burden reduces the lifetime of CH_4 (Equation R1), a potent greenhouse gas and a major contributor to global warming (Naik et al., 2013; Banerjee et al., 2014;

https://doi.org/10.5194/egusphere-2024-3087
Preprint. Discussion started: 5 November 2024

Murray et al., 2021). By improving the parameterization of LNOx in CHIMERE, this study strengthens our understanding of tropospheric chemistry and the dynamics of trace gases.

$$CH_4 + OH \rightarrow CH_3 + H_2O \quad \text{(R1)}$$

Hence the specific objectives of the study are, (i) to assess and improve the lightning flash parameterization with the CHIMERE model using the CTH scheme; (ii) to evaluate the effect of LNOx emissions on tropospheric O_3 and (iii) the influence on the OH burden and lifetime of CH_4 quantified against the chemical loss. The detailed methodology is provided in Section 2. An analytical evaluation of the simulated results have been carried out and presented in the following sections.

2 Method of study

2.1 CHIMERE model configuration and experimental set-up

In this study, simulations are carried out with the CHIMERE chemistry-transport model (version 2023r2; Menut et al., 2024) over the domain of northern hemisphere (NH) expanded from 0°–90°N, at a horizontal resolution of 100×100 km^2. Here, meteorological fields are forced externally to CHIMERE with a 3-hourly forecast dataset from European Centre for Medium-Range Weather Forecasts (ECMWF)– Integrated Forecasting System (IFS) (https://www.ecmwf.int/en/forecasts/datasets, last access: 16 May, 2024). Simulations are done in twenty vertical levels in σ-pressure coordinates ranging from surface (998 hPa) to 200 hPa over one year (January–December, 2018) with a spin-up time of 15 days. The MELCHIOR2 scheme is used for chemical mechanisms. The CHIMERE model employs a 10-bin logarithmic sectional size distribution ranging from 0.01 to 40 μm. Fields of chemical concentration are calculated with a time-step of few minutes, using an adaptive time-step, to ensure that the Courant-Friedrichs-Lewy (CFL) stability criterion is satisfied (Menut et al., 2021). The chemical speciation of aerosols includes elemental carbon (EC), primary organic aerosols (POAs), secondary organic aerosols (SOAs), nitrates, sulfates, ammonium, dust, sea salt, and primary mineral particulate matter (PPM). Boundary and initial conditions are derived from climatological simulations of the global chemistry-transport model Laboratoire de Météorologie Dynamique General Circulation Model coupled with Interaction with Chemistry and Aerosols (LMDz-INCA3) for gaseous and particulate species (Hauglustaine et al., 2014), and from GOCART for dust concentrations (Chin et al., 2002). Biogenic emissions are provided by a reduced online version of the Model of Emissions of Gases and Aerosols from Nature (MEGAN) model (version 2.10) (Guenther et al., 2012). Mineral dust and sea-salt emissions are calculated using the schemes of Alfaro and Gomes (2001) and Monahan (1986), respectively. The formation of SOA is as described in Pun and Seigneur (2007) and Bessagnet et al. (2008). The aerosol dynamic processes, such as condensation, coagulation, wet and dry deposition, absorption, and scavenging, are incorporated into the model (Menut et al., 2021). The mixing state is considered internal homogeneous aerosol mixing (Menut et al., 2013). The online calculations for radiation and photolysis are incorporated using the FastJX module (Wild et al., 2000; Mailler et al., 2016). The horizontal transport is solved with the van Leer (1977) scheme and vertical using Després

https://doi.org/10.5194/egusphere-2024-3087
Preprint. Discussion started: 5 November 2024

and Lagoutière (1999) scheme (Lachatre et al., 2020). Boundary layer height and vertical diffusion are calculated by the parametrization proposed by Troen and Mahrt (1986) and deep convection fluxes are estimated using the Tiedtke (1989) scheme. Gaseous and aerosol species undergo dry or wet deposition and fluxes are calculated using the Wesely (1989) and Zhang et al. (2001) parameterization schemes. With access to anthropogenic and biogenic emissions, CHIMERE simulates 3D concentration for a range of gaseous and size-resolved particulate species, based on the chosen chemical scheme.

Simulations carried out for this study are (i) not including LNOx emissions (experiment: noLNOx), (ii) including LNOx emissions estimated with parameterization based on cloud top height (CTH) developed by Price and Rind (1992), applying a correction factor over the land grids (experiment: wLNOx). Anthropogenic emissions in the model are incorporated from Copernicus Atmosphere Monitoring Service (CAMS)-global and fire emissions are from CAMS Global Fire Assimilation System (GFAS, https://atmosphere.copernicus.eu/global-fire-emissions, last access: 16 May, 2024).

2.2 Estimation of LNOx emissions

The LNOx emission calculation is done as per the CTH scheme (Price and Rind, 1992). Derived from the theories advanced by Vonnegut (1963) and Williams (1985), Price and Rind formulated the CTH parameterization, wherein the flash rate is contingent upon the cloud top height (H). The distinct relationships governing flash rates over land and ocean are delineated as follows:

$$\begin{aligned} F_l &= a \times H^{4.9} \\ F_o &= b \times H^{1.73} \end{aligned} \tag{1}$$

Here, a and b are constants (values are provided in Table 1), H represents the cloud-top height above the ground level in km, estimated based on the convection scheme of the model. F denotes the total flash frequency in flash number min^{-1} 25 km^{-2}, with subscripts 'l' and 'o' indicating land and ocean, respectively (Menut et al., 2020a). The distinction between land and ocean is employed to incorporate the disparity in updraft velocity over these two surface types. For instances where the cloud depth is less than 5 km, the flash value is set to zero, a criterion based on the data range utilized in developing the relationship by Price and Rind (1992). It's noteworthy that Price and Rind (1994) formulated an equation to adapt the above equations to various model resolutions. The scaling factor (C) determined to accommodate the model grid cell size is outlined as follows:

$$C = 0.97241e^{0.048203 \times \Delta x \times \Delta y} \tag{2}$$

Here, the product of longitude and latitude resolution, denoted as Δx $\times$ Δy, is measured in degrees^2. This factor typically remains close to 0.97, and its impact on the results is generally minimal, especially when compared to the uncertainties of other parameters, except at very coarse resolutions. These uncertainties are typically offset by adjustment factors, that align the model more closely with observations (Gordillo-Vázquez et al., 2019). For example, in the study by Finney et al. (2014),

https://doi.org/10.5194/egusphere-2024-3087
Preprint. Discussion started: 5 November 2024

a scaling factor of 0.05 has been applied to match the estimated flash rate to the satellite-based observation. In our study, we observe a highly overestimated flash rate compared to satellite measurements, over the land grids from a preliminary simulation, estimated based on the formulations by Price and Rind (1992). In this regard it is also to be noted that, satellites are unable to capture all the flashes, therefore providing minimized values of flash rate (Erdmann et al., 2020; Zhang et al., 2023). Considering the overestimation in the modelled flash rate and the uncertainty in satellite-based observations, we have applied a factor of 1/5 to constant 'a' in Equation 1 over the land grids, in experiment wLNOx, to reconcile the modelled lightning flash rate to the satellite observations (Table 1).

Table 1. Values of constants in Equation 1

constants	Price and Rind (1992)	present study (experiment: wLNOx)
a	3.44×10^{-5}	6.88×10^{-6}
b	6.40×10^{-4}	6.40×10^{-4}

For each grid-cell, the relative percentage of sea (x_{sea}) is determined using the land-sea mask from the land use database (Menut et al., 2020a). The flash frequency is then calculated as follows:

$$F = \frac{C \times (x_{\text{sea}} \times F_o + (1 - x_{\text{sea}}) \times F_l)}{25} \tag{3}$$

Here, F represents total flash rate as flash number mn^{-1} km^{-2}. The empirically derived formula used to determine the relative proportion of 'cloud to ground (CG)' flashes in a single thunderstorm is initially based on the cloud ice depth (H_f) (Price and Rind, 1993). H_f is estimated in km as,

$$H_f = -6.64 \times 10^{-5}|L|^2 - 4.73 \times 10^{-3}|L| + 7.34 \tag{4}$$

Here, L represents the latitude in degrees. Parameter β is calculated as follows:

$$\beta = 0.021H_f^4 - 0.648H_f^3 + 7.49H_f^2 - 36.54H_f + 64.09 \tag{5}$$

where, β varies between 1 to 50 for H_f varies between 5.5 to 14 km to prevent unrealistic values. The relative part of CG in the total (in cloud (IC) + CG) is denoted by p (Equation 6).

$$p = \frac{1}{1 + \beta} \tag{6}$$

https://doi.org/10.5194/egusphere-2024-3087
Preprint. Discussion started: 5 November 2024

Finally, with the flash frequency and the vertical distribution of CG and IC for each flash, the NO emission is estimated in molecules flash^{-1} (Equation 7; Price et al., 1997a).

$$\begin{aligned} P(\text{CG, NO}) &= 6.7 \times 10^{26} \\ P(\text{IC, NO}) &= 6.7 \times 10^{25} \end{aligned} \tag{7}$$

The NO_2 emissions are assumed to be 10% of the NO emissions. However, CTH parameterization simplifies the vertical structure of the emissions, considering the emissions to be evenly distributed over an altitude range, i.e., the CG flux from the surface to H_f and the IC value from H_f to the cloud top (Menut et al., 2020a).

2.3 Lifetime of CH_4 due to chemical loss

The loss in tropospheric methane (CH_4) is primarily (90%) due to oxidation by hydroxyl radicals (OH, Equation R1)(Ghosh et al., 2015). The estimation of tropospheric chemical loss rate of CH_4 is as follows (in molecules cm^{-3} s^{-1}) (Zhao et al., 2023):

$$\text{rate} = k(T)[\text{CH}_4][\text{OH}] \tag{8}$$

where, [CH_4] and [OH] are the concentrations of CH_4 and OH (in molecules cm^{-3}). [OH] is taken from simulation in CHIMERE from our study, whereas [CH_4] is from chemical boundary conditions. The reaction rate (k(T) in cm^3 molecule^{-1} s^{-1}) is temperature (T) dependent (Burkholder et al., 2019) and is represented in (Menut et al., 2013),

$$k(T) = 2.3 \times 10^{-12} \exp\left(-\frac{1765}{T}\right) \tag{9}$$

The total tropospheric chemical loss of CH_4 (L in Tg yr^{-1}) is estimated as,

$$L_{\text{CH}_4} = \int_{\text{V}} k(T)[\text{CH}_4][\text{OH}]\, dV \tag{10}$$

dV is the differential volume element in the troposphere. The lifetime of CH_4 (τ_{CH_4} in year) is expressed as,

$$\tau_{\text{CH}_4} = \frac{B_{\text{CH}_4}}{L_{\text{CH}_4}} \tag{11}$$

https://doi.org/10.5194/egusphere-2024-3087
Preprint. Discussion started: 5 November 2024

Here, B_{CH_4} is the annual tropospheric burden (in Tg) of CH_4. Note that, all the calculations in our study are done for NH.

2.4 Observation data for evaluation

Flash rate from Lightning Imaging Sensor (LIS) on the International Space Station (ISS) platform, is used for evaluating flash rate estimated with the model. ISS-LIS optically detects lightning flashes that occur within its field-of-view during both day and night with storm-scale (4 km × 4 km) horizontal resolution (Blakeslee et al., 2020). ISS-LIS allows expansion of the long-term global lightning climatology from space and extends the global record to higher latitudes (±55°). The flash rate data from ISS-LIS is re-gridded to the resolution of simulated fields before comparison. The simulated O_3 and NO_2 mixing ratio is compared with ground-based observation data from OpenAQ (https://openaq.org, last access: 5 July, 2024; Hasenkopf et al., 2015), U.S. Environmental Protection Agency (EPA, https://www.epa.gov, last access: 5 July, 2024), European Environment Agency (EEA, https://www.eea.europa.eu, last access: 5 July, 2024), Environment and Climate Change Canada (ECCC) data catalogue (https://data-donnees.az.ec.gc.ca, last access: 5 July, 2024), Subsistema de Informacion de Calidad del Aire (SISAIRE, http://sisaire.ideam.gov.co, last access: 5 July, 2024) and China National Environmental Monitoring Centre (CNEMC, https://quotsoft.net/air/, last access: 5 July, 2024; Dufour et al., 2021), collected over the study period. The total number of observation stations over the NH are mentioned in Table 3. The evaluation of simulated data is done with the statistical analyses estimating the mean absolute bias (MAB), normalised mean error (NME), and root mean square error (RMSE), using the annual mean of O_3 and NO_2 mixing ratio. For evaluating the vertical profile of O_3, altitudinal data measured by ozone sonde, launched on small balloons, are downloaded from the World Ozone and Ultraviolet Radiation Data Centre (WOUDC, https://woudc.org/data, last access: 5 July, 2024). Ozone sonde data from 122, 977 and 121 stations are collected, respectively, over the tropical (0°–30°N), mid-latitudes (30° N–60° N) and polar region (60° N–90° N).

3 Results and Discussions

3.1 Evaluation of lightning flash rate and NOx emissions from lightning

The spatial distribution of average flash rates during the period of May–August, is presented in Figures 1b from experiment wLNOx. wLNOx is the simulation with CTH scheme applying a correction factor of 1/5 over the land grids. Keeping the cruciality of representing the flash numbers in mind, specifically during the period of May–August, showing highest flash rates over NH (Christian and Petersen, 2005; Allen et al., 2010), the evaluation of the modelled flash rate for this period is done. The annual mean of flash rate from experiment wLNOx is also shown in Figure 1d. As observed from our study, warm tropical regions (0°–30°N), especially central Africa, south America, India and south China are the regions with high lightning flash rate due to large convective activity, followed by the mid-latitude region (30° N–60° N). The generation of LNOx has been reported to be significant in the tropics and mid-latitudes (Allen et al., 2010). The averaged annual flash rate from wLNOx experiment is observed as 0.8–1.5 flashes km^{-2} day^{-1} over most of the tropical lands (Figure 1d). South Asia, including India and south China, has been reported exhibiting the greatest seasonal and interannual variation in lightning activity (Pawar et al.,

https://doi.org/10.5194/egusphere-2024-3087
Preprint. Discussion started: 5 November 2024

2012a; Xu et al., 2023). The spatial pattern of flash rate is in agreement with the ISS-LIS satellite-based observation (Figures 1a and 1c) and other model-based studies (Finney et al., 2014, 2016a; Murray, 2016), but shows a pronounced bias over the tropical lands. The large bias over tropics is also observed in other model-based studies (Murray et al., 2012; Finney et al., 2014). After applying the correction factor over lands in experiment wLNOx, the bias is reduced to a factor ≈6 as averaged over the tropical lands for the period of May–August and ≈5 for annual mean of flash rate (Table 2). The bias over tropics is possibly due to the limitation of the CTH scheme by tropopause height which is highest at equator and decreases away from the equator (Finney et al., 2014). Uncertainty in flash rate data from ISS-LIS is also considerable in this context. The patches of high flash rate over the central region of Canada, United states of America (USA) and north-eastern region of China are found missing in the modelled flash rate (Figures 1b and 1d). The simulated flash rate over the mid-latitude lands and ocean is relatively well-matched with the ISS-LIS observations, however shows an overestimation by factors 3–5.75 over the tropical oceans (Table 2). Nevertheless, controversies still remain on estimating lightning flashes over ocean and inconsistancies are found in the equation for ocean, developed by Price and Rind (1992) (Michalon et al., 1999; Boccippio, 2002; Luhar et al., 2021). The average flash rate during the period of May–August, is found to be twice the annual mean of flash rate from ISS-LIS-based observations, while it is higher by a small fraction (5%–30%) in comparison to the annual mean rate from our study (experiment wLNOx). The seasonality is however not well captured in the simulation, causing an overall high flash rate.

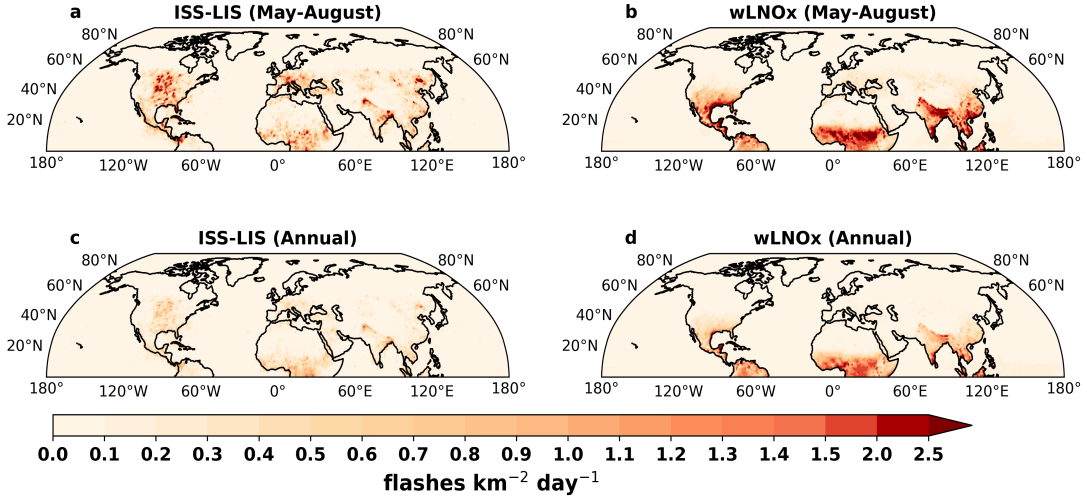

Figure 1. Spatial distribution of flash rate (a–b) averaged over the period of May–August, from (a) ISS-LIS satellite-based observations and (b) experiment wLNOx; (c–d) averaged over the year, from (c) ISS-LIS satellite-based observations and (d) experiment wLNOx.

The estimated annual NO emission from lightning in experiment wLNOx is 8.82 Tg N yr^{-1} over the NH. Recent studies estimate that global NO emissions from lightning (LNO) to be typically within the range of 2 to 8 Tg N yr^{-1} (Schumann and Huntrieser, 2007; Finney et al., 2016b; Nault et al., 2017), but may vary within a wide range up to 25 Tg N yr^{-1} (Price et al., 1997a, b). The study by Luhar et al. (2021) shows that, the LNO emissions are almost equally contributed from both northern and southern hemispheres, while estimated in a global chemistry-climate model, applying the CTH scheme. Considering this,

https://doi.org/10.5194/egusphere-2024-3087
Preprint. Discussion started: 5 November 2024

Table 2. Comparison of modelled flash rate to ISS-LIS based observation over land and ocean

	Ratio of modelled to observed flash rate from experiment wLNOx, averaged over the period			
	May–August		annual	
	0°–30° N	30° N–55° N	0°–30° N	30° N–55° N
Land	6.10	2.03	5.23	1.64
Ocean	3.17	0.52	5.75	0.46

the LNO emission estimated in our study lies within the range of global LNO emissions as mentioned above. CTH scheme though oversimplifies the complex interactions and distributions of charge that contribute to lightning production (Price and Rind, 1992; Finney et al., 2014). It does not account for the complex microphysical processes, storm dynamics and presence of ice particles as well (Price and Rind, 1992), explaining the insufficiently reproduced seasonality in the flash rate in our study. The limitations further motivate us to conduct a study in future, applying new schemes that include more parameters in order to represent the average and variability of flash numbers better.

3.2 Impact of lightning on surface-level O_3 and precursor gases

The underestimation in emissions is a major source of uncertainty in simulated fields, highlighting the need for a more accurate representation of emissions in models. LNOx is one of such uncertain emissions, that has been incorporated into models over the past few decades (Allen et al., 2010; Banerjee et al., 2014; Finney et al., 2016a; Kang et al., 2019, 2020). In this study, we have conducted a simulation with LNOx emissions in a chemistry transport model CHIMERE and the effect on surface level O_3 and nitrogen dioxide (NO_2) over NH is analysed in this section.

The spatial distribution of the annual mean of O_3 mixing ratio and NO_2 at the surface from experiment wLNOx and changes in the mixing ratio due to inclusion of LNOx (ΔO_3 and ΔNO_2), are presented in Figures 2a, 2d and 2b, 2e, respectively. Other than natural sources (e.g., lightning), emissions from fossil fuel combustion for transportation, industrial activities, energy generation and biomass burning also have a profound influence on tropospheric O_3 and NO_2 concentrations (Lelieveld and Dentener, 2000; van der A et al., 2008; Butler et al., 2020). In our study, the O_3 mixing ratio at the surface represents a spatial variation with higher values ranging between 40–60 ppbv over the tropics and mid-latitudes up to 50°N, specifically over the lands, being almost 1.5–2 times of that observed over the rest part of NH. The NO_2 at the surface, is within a range of 0.5–2 ppbv over most parts of the NH showing higher magnitudes over USA, western Europe, India, eastern China and Japan (5–10 ppbv). To indicate the impact of LNOx emissions on changes in surface-level O_3 and NO_2, annual mean of mixing ratio obtained from experiment wLNOx is compared with respect to that from noLNOx. The positive and negative values of ΔO_3 and ΔNO_2 depict an increase and decrease, respectively, in surface mixing ratio (Figures 2b and 2e). The study shows an overall increase in surface O_3 by 2–5 ppbv over most parts of the tropical lands and mid-latitudes up to 50°N (Figure 2b), while the increase is almost negligible over 50°–90°N ($<$1 ppbv). A comparatively larger increase by 5–10 ppbv is observed

https://doi.org/10.5194/egusphere-2024-3087
Preprint. Discussion started: 5 November 2024

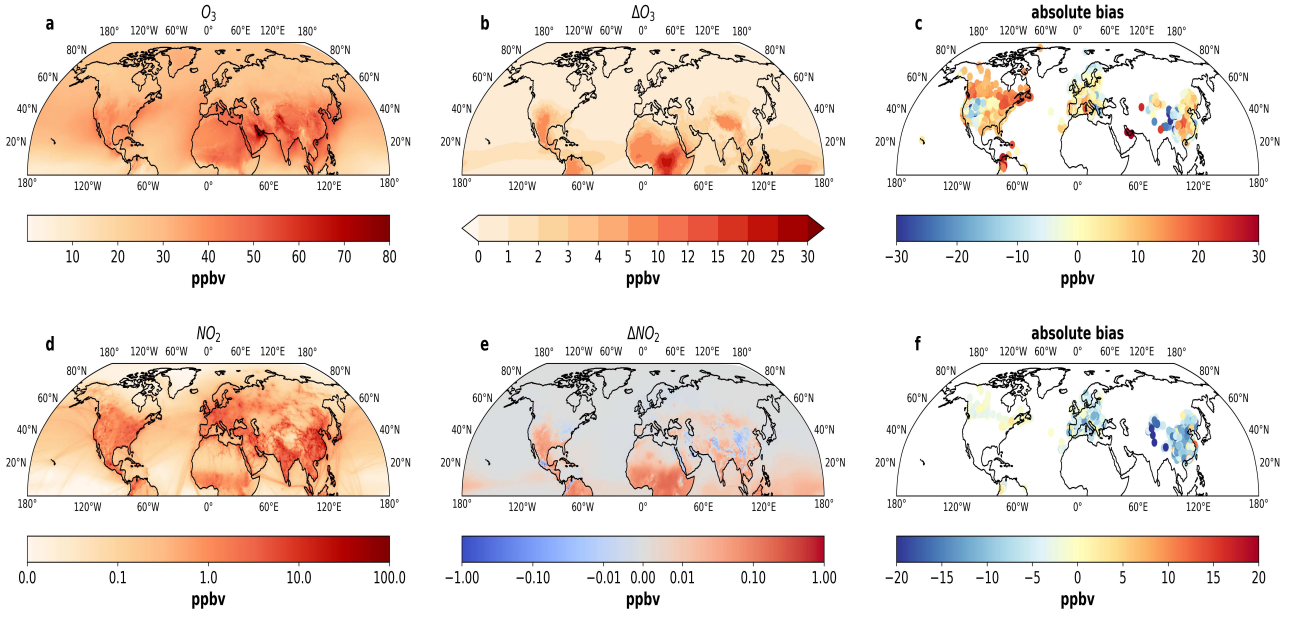

Figure 2. (a, d) Spatial distribution of annual mean mixing ratio in ppbv at the surface over NH from experiment wLNOx for (a) O_3, (d) NO_2; (b, e) changes in mixing ratio at the surface due to inclusion of LNOx emissions for (b) O_3, (e) NO_2, positive and negative values show an increase and decrease, respectively; (c, f) absolute bias in simulated mixing ratio at surface at stations for (c) O_3, (f) NO_2, positive and negative values of absolute bias represent that modelled O_3 and NO_2 are higher and lower than the measurements, respectively.

over tropical parts of America and Africa and the Tibetan Plateau, but is particularly noteworthy (10–25 ppbv) over the central part of Africa, which is a hotspot location with high lightning flash rate (Figure 1d). Unlike O_3, NO_2 exhibits both increase and decrease in mixing ratio at the surface as an effect of lightning (Figure 2e), but by a very weak value (0.01–0.1 ppbv). While the increase is observed over most of the tropical and mid-latitude lands, a decrease in NO_2 mixing ratio is also there at high altitude Himalayan region at north of India, northern China, south-west Asia and a few areas over Canada. O_3 and NO_2, both exhibit a slight increase over the Atlantic, Indian and Pacific Oceans in the tropics. The magnitudes and spatial patterns of ΔO_3 and ΔNO_2 from our study bear a resemblance to those from recent studies (Murray, 2016; Li et al., 2022; Cheng et al., 2024). The impact on surface O_3 and NO_2 concentrations is a localized effect of thunderstorms, crucially influenced by the specific photochemical conditions in the area (Murray, 2016). An increase in surface O_3 levels due to LNOx suggests the NOx concentration to be below the titration threshold (Pawar et al., 2012b).

Figures 2c and 2f represent the absolute bias in the simulated annual mean of O_3 and NO_2 at the surface from experiment wLNOx, compared to the observations at stations. The simulated O_3 and NO_2 mixing ratio is close enough to the observations at most of the stations over Europe and China, and also over the USA for O_3 and Canada and south America for NO_2. Higher bias for O_3 is, nonetheless, observed at stations over Canada, South America and northern and eastern China. The statistical analyses are done and presented in Table 3. The agreement between simulated and observed O_3 is considered good, as indicated by low values of RMSE (10.90 ppbv), MAB (5.63 ppbv), and NME (13.95%). In contrast, the comparison for

https://doi.org/10.5194/egusphere-2024-3087
Preprint. Discussion started: 5 November 2024

NO_2 is moderately acceptable, with a slightly higher NME of 27.46%. However, the inclusion of LNOx does not significantly impact the statistical scores when comparing surface mixing ratios with observations. A detailed analysis of the altitude-wise changes in the mixing ratio of O_3, due to the impact of LNOx, is therefore necessary and is discussed in the next section.

Table 3. Statistical analysis comparing simulated mixing ratio at surface to the ground-based observations for O_3 and NO_2

	Mean observed surface conc. over NH (ppbv)	Total number of stations	noLNOx RMSE (ppbv)	noLNOx MAB (ppbv)	noLNOx NME (%)	wLNOx RMSE (ppbv)	wLNOx MAB (ppbv)	wLNOx NME (%)
O_3	32.48	5185	10.64	4.70	13.45	10.90	5.63	13.95
NO_2	13.3	3857	9.09	6.28	27.44	9.10	6.27	27.46

The positive and negative values of MAB represent respectively, modelled fields are higher and lower than the measurements.

3.3 Vertical distribution of O_3: effect of LNOx

The increase in the annual mean of O_3 mixing ratio, due to the inclusion of LNOx in simulation wLNOx, with respect to that from simulation noLNOx, averaged over four altitude bands (998–900, 900–750, 750–500 and 500–200 hPa) is presented in Figure 3. The highest increase in simulated O_3 is observed at the altitude band 750–500 hPa, specifically over the tropics, by 10–20 ppbv. 6–12 ppbv increase over the tropics is also observed at the altitude bands 750–500 hPa and 500–200 hPa (upper troposphere). The increase is maximum over the northern part of South America, central Africa, the eastern part of China and the Maritime Continent in south-east Asia (Indonesia, Philippines and Malaysia). The above-mentioned regions with large increases in O_3, identified for all the altitude bands, are observed as regions with the largest convection depth and LNOx emissions (Banerjee et al., 2014). The changes in O_3 mixing ratio are low to negligible over mid-latitudes (30° N–60° N) and polar region (60° N–90° N). The percentage increase in the annual mean of O_3 mixing ratio due to the inclusion of LNOx in the model, at selected latitude and altitude bands, is also presented in Table 4. Inclusion of LNOx in the model calculation, overall increases tropospheric O_3, while it is considerably high in the mid and upper troposphere (750–200 hPa), where O_3 is elevated by 20%–35%, especially over the tropics, as the maximum lightning discharge is found over the tropical mid to upper troposphere (Luhar et al., 2024). A moderate (6%–9%) to low (1%–2%) increase in mid and upper tropospheric O_3 is observed over mid-latitudes followed by the polar region. The tropospheric O_3 burden over NH is 133.63 Tg as estimated from the simulation wLNOx and is increased by 15% with respect to noLNOx simulation (Table 6). The estimated O_3 burden from our study is close enough but slightly underestimated in comparison to the global burden calculated in previous modeling studies (308–337 Tg; Young et al. (2013); Banerjee et al. (2014); Luhar et al. (2021)).

Figure 4 represents the vertical profile of the annual mean of O_3 mixing ratio from noLNOx and wLNOx simulations and their comparison with the ozone sonde measurements, averaged for the stations over the latitude bands 0°–30° N, 30° N–60° N and 60° N–90° N. The simulated O_3 mixing ratio does not vary significantly up to 500 hPa, as also presented in Table 4, whereas an increase in O_3 mixing ratio from the ozone sonde is observed along with increasing altitude. The upper tropospheric O_3 mixing ratio is slightly higher (by 15%–20%) than that observed at surface over the tropics, while it is 2–4 times higher over the mid-latitudes and polar region (Table 4). The upper tropospheric O_3 over the polar region is also almost twice that

https://doi.org/10.5194/egusphere-2024-3087
Preprint. Discussion started: 5 November 2024

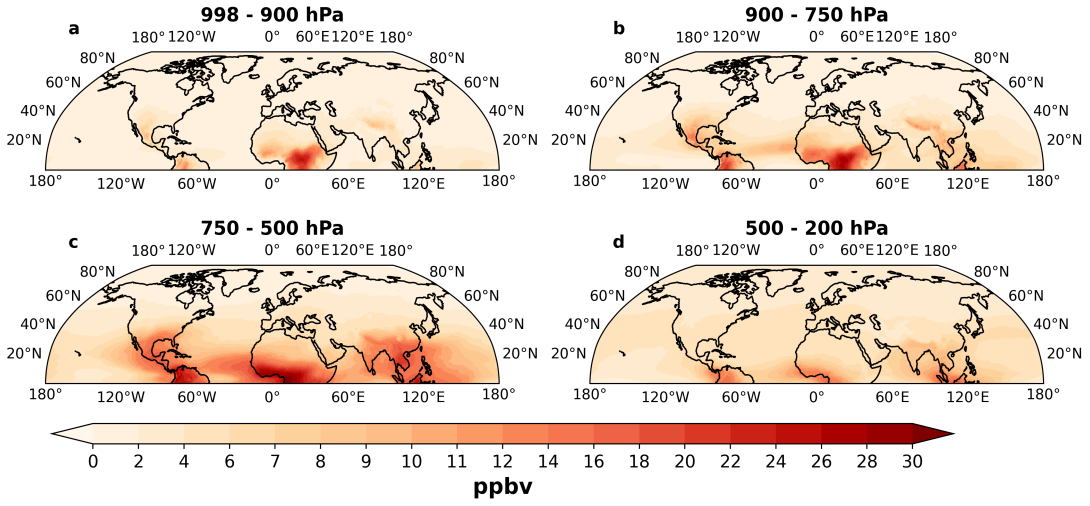

Figure 3. Changes in the annual mean of O_3 mixing ratio due to inclusion of LNOx emissions at the altitude bands of (a) 998–900 hPa, (b) 900–750 hPa, (c) 750–500 hPa and (d) 500–300 hPa; positive and negative values represent the increase and decrease in the O_3 mixing ratio, respectively.

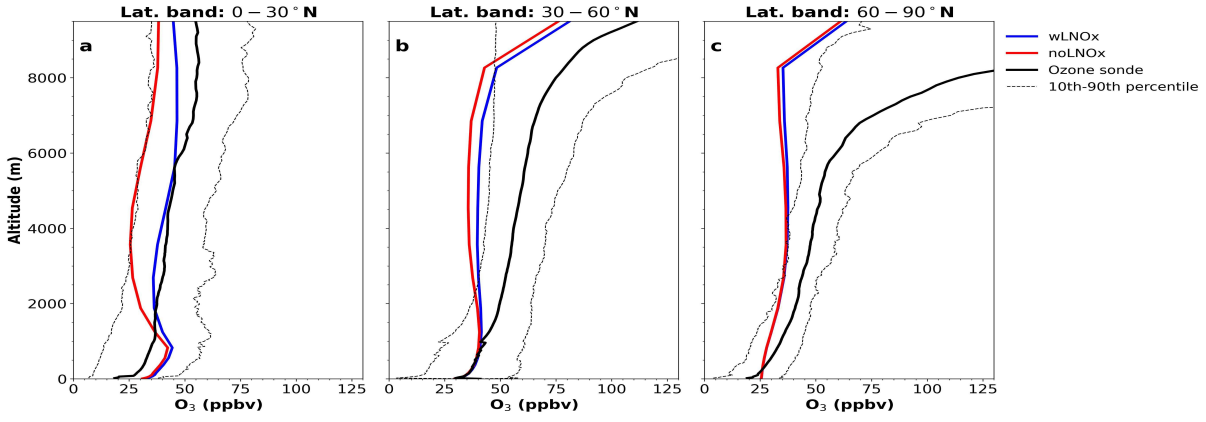

Figure 4. Vertical profile of annual mean of O_3 mixing ratio from noLNOx (red solid line) and wLNOx (blue solid line) simulations and comparison with the ozone sonde measurements (black solid line), averaged for the stations over the latitude bands (a) 0°–30° N, (b) 30° N–60° N and (c) 60° N–90° N; the black dashed lines indicate the 10 and 90 percentiles of the ozone sonde data.

over the tropics (Table 4). It is visible in Figure 4, that the simulated O_3 mixing ratio from the wLNOx experiment, represents the same from ozone sonde adequately well, in mid to upper troposphere over tropics and near-surface over mid-latitudes and polar region. The simulated O_3 over the tropics, mostly lies between the 10th and 90th percentiles of the ozone sonde data, showing that the model predictions are within a reasonable range of the observed variability. However, simulated O_3 highly deviates from the ozone sonde measurements above 900 hPa (around 1000 m) over mid-latitude and polar regions. The sharp increase in O_3 above 900 hPa, is not captured in the simulated O_3 profile, even after including LNOx in the model calculation,

https://doi.org/10.5194/egusphere-2024-3087
Preprint. Discussion started: 5 November 2024

explaining the underestimation of tropospheric O_3 burden in NH as mentioned above. The O_3 in the model consistently falls below the 10th percentile of the ozone sonde data at the free troposphere over mid-latitudes and the polar region, suggesting a systematic underestimation in the simulated O_3, specifically in polar region. The absolute bias in simulated O_3 from simulations noLNOx and wLNOx, with respect to observed data from ozone sonde at selected latitude and altitude bands, is also presented in Table 4. The absolute bias in simulated O_3 in the mid to upper troposphere over tropics and mid-latitudes is reduced due to inclusion of LNOx in the model, but still shows an underestimation. The bias reduction is significantly larger over the tropics in comparison to mid-latitudes. It is evident that, the O_3 production efficiency from LNOx is comparatively higher in the mid to upper troposphere due to lower temperature, which is favourable for the longer lifetime of NOx and O_3 (Finney et al., 2014). The high underestimation in the simulated upper tropospheric O_3 mixing ratio, especially over mid-latitudes and polar regions, is possibly due to inadequate vertical mixing and representation of convection in the model and lack in stratosphere-troposphere exchange (Allen et al., 2010, 2012).

Table 4. Details of annual mean O_3 from experiment 'wLNOx', its changes due to inclusion of LNOx and evaluation of simulated O_3 from experiments 'noLNOx' and 'wLNOx' w. r. t. observed data from ozone sonde at selected latitude and altitude bands

Latitude band	0°–30° N	30° N–60° N	60° N–90° N	0°–30° N	30° N–60° N	60° N–90° N	0°–30° N	30° N–60° N	60° N–90° N
Altitude band (hPa)	Annual mean O_3 from 'wLNOx' in ppbv (ΔO_3* in %)			mean absolute bias in ppbv (correlation coefficient) in simulated O_3 from expt. 'noLNOx'**			mean absolute bias in ppbv (correlation coefficient) in simulated O_3 from expt. 'wLNOx'**		
500–200	46.5 (19.6)	77.3 (5.8)	90.6 (2.3)	−13.69 (0.39)	−56.90 (0.80)	−146.38 (0.82)	***−6.04*** (0.42)	**−52.63** (0.79)	−144.32 (0.82)
750–500	39.8 (35.0)	40.1 (9.2)	36.1 (1.2)	−12.00 (0.61)	−18.43 (0.20)	−11.71 (0.36)	***−1.68*** (0.62)	**−15.04** (0.38)	−11.27 (0.39)
900–750	39.8 (10.6)	41.4 (2.6)	31.3 (0.1)	−0.97 (0.81)	−6.73 (0.65)	−7.16 (0.29)	2.85 (0.80)	−5.66 (0.66)	−7.13 (0.29)
998–900	39.8 (3.2)	36.05 (1.2)	25.8 (0.1)	11.52 (0.77)	−0.65 (0.66)	0.61 (−0.08)	12.76 (0.76)	−0.21 (0.66)	0.62 (−0.08)

*ΔO_3 represents changes in O_3 from experiment 'wLNOx' w. r. t. that from experiment 'noLNOx'; positive and negative values represent the increase and decrease in O_3 mixing ratio, respectively.
**Reduction in absolute biases in the experiment 'wLNOx' w.r.t. 'noLNOx' (i) ≥3 ppbv and ≤6 ppbv: bold (for lower bias); (ii) ≥6 ppbv: bold, italics (for lower bias); positive and negative values of absolute bias show that the simulated O_3 is higher and lower than the measurements, respectively; correlation between the simulated and observed O_3 mixing ratio is estimated over space and time, aggregating stations in each latitude-altitude band and comparing values over time.

The correlation between simulated and ozone sonde-derived O_3 (represented in Table 4) is strong only at lower altitudes over tropics and mid-latitudes and at upper troposphere over mid-latitudes and polar region and is not much affected due to the inclusion of LNOx. The correlation is weak in the mid to upper troposphere over the tropics despite of improvement in O_3 mixing ratio, suggesting that the model is not accurately capturing the observed variations and patterns in the O_3 data. This may indicate a limitation in the representation of the transport processes in model and a lack in emissions, especially during the biomass-burning seasons (von Kuhlmann et al., 2003).

3.4 Impacts on tropospheric OH burden and CH_4 lifetime

In the present study, we also have evaluated the effects of LNOx on tropospheric chemistry in terms of changes in the burden of a major oxidant (OH) and the lifetime of trace gas CH_4. Table 5 illustrates the concentration of OH from experiment wLNOx and the increase in concentration of OH, averaged over selected latitude and altitude bands. The highest OH concentration is observed at the tropical mid troposphere (21–27 $\times$ 10^5 molecules cm^{-3}). The OH concentration over the tropics is almost 2–3

https://doi.org/10.5194/egusphere-2024-3087
Preprint. Discussion started: 5 November 2024

times and 8–10 times higher than that over mid-latitudes and polar regions, respectively. The OH concentration from our study is close enough to those values obtained in a multi-model study by Naik et al. (2013), but shows a higher OH concentration at tropical mid-troposphere than the surface, unlike the multi-model study. While the studies by Naik et al. (2013); Luhar et al. (2021), exhibit higher OH concentration at the surface than mid and upper troposphere, on the contrary higher concentration is observed in upper troposphere from the study by Banerjee et al. (2014). The annual mean OH concentration over NH from our study is 14 $\times$ 10^5 molecules cm^{-3}, which is around 19% higher than that obtained from noLNOx simulation (Table 6). The annual average OH concentration is higher by 26% in comparison to the multi-model mean obtained from ACCMIP simulations (11.1$\pm$1.8 $\times$ 10^5 molecules cm^{-3}; Naik et al., 2013; Voulgarakis et al., 2013). We find an increase in OH concentration due to LNOx, which is again the largest over mid and upper troposphere at tropics (59%–65%), followed by mid-latitude and polar regions (Table 5). A warmer atmosphere and high humidity influence an increase in OH and a faster OH to CH_4 reaction, causing a shorter CH_4 lifetime (Voulgarakis et al., 2013). The OH burden over NH is increased to 0.091 Gg, from 0.065 Gg, due to the inclusion of LNOx (Table 6). In our study, we have estimated CH_4 lifetime (τ_{CH_4}) due to chemical loss, mainly due to reaction with OH and the average lifetime over NH is 4.89 years, as obtained from experiment wLNOx. The lifetime of CH_4 is reduced by 24% compared to the estimate from the noLNOx simulation (Table 6), evidencing that the increase in OH burden due to LNOx decreases the CH_4 lifetime. The CH_4 lifetime as estimated from previous modeling studies, is within a range of 7–14 years (Naik et al., 2013; Lelieveld et al., 2016) and is visibly underestimated in our study. It is to be noted in this regard that, the CH_4 anthropogenic emissions are not taken into account in the model and CH_4 concentration comes from chemical boundary conditions. Hence, it is necessary to evaluate the sensitivity of CH_4 lifetime estimates toward the initial chemical boundary conditions. Additionally, there is a need for further investigation into the source and sink pathways of OH in the CHIMERE model to improve the estimation of the OH burden and CH_4 lifetime.

Table 5. OH concentration averaged over selected latitude and altitude bands for simulations wLNOx and percentage increase in OH concentration w. r. t. noLNOx

Latitude band	0°–30° N	30° N–60° N	60° N–90° N	0°–30° N	30° N–60° N	60° N–90° N
Altitude band (hPa)	OH concentration (10^5 molecules cm^{-3}) from wLNOx			ΔOH† (%)		
500–200	15.06	6.48	2.31	59.36	24.37	15.5
750–500	27.59	10.23	2.79	65.11	29.16	7
900–750	21.24	11.08	2.95	29.19	9.05	0
998–900	18.27	13.28	2.56	8.62	2.07	0

$^\dagger\Delta$OH represents changes in OH from experiment 'wLNOx' w. r. t. that from experiment 'noLNOx'; positive and negative values represent the increase and decrease in OH concentration, respectively.

Conclusion

In the present study, NOx from lightning (LNOx) has been incorporated in the chemistry-transport model CHIMERE and its effect on tropospheric ozone (O_3) is studied. The LNOx is estimated with a classical parameterization based on cloud top

https://doi.org/10.5194/egusphere-2024-3087
Preprint. Discussion started: 5 November 2024

Table 6. Tropospheric O_3, OH burden and CH_4 lifetime from simulation experiments

	noLNOx	wLNOx
O_3 burden (Tg)	116.53	133.63
OH concentration (molecules cm^{-3})	11.72×10^5	14.01×10^5
OH burden (Gg)	0.065	0.091
CH_4 lifetime due to chemical loss (yr)	6.45	4.89

height (CTH) developed by Price and Rind (1992). A correction factor of 1/5 is applied over the land grids to exhibit the modelled flash rate close to the satellite-based measurements (experiment: wLNOx). The estimated annual mean of flash rate from our study is highest over tropical lands (0.8–1.5 flashes km^{-2} day^{-1}) and provides 5–6 times higher values over the tropics, in comparison to observations. The total NO emissions from lightning (LNO) is estimated as 8.82 Tg N yr^{-1} over the northern hemisphere (NH) and lies within the wide range of model-estimated LNO emissions from previous studies. The high uncertainty in modelled flash rates, LNOx emissions and insufficiently simulated seasonality in flash rate, estimated using the over-simplified CTH parameterization scheme, drive us to investigate more recent parameterization methods for lightning.

To examine the effects of LNOx on tropospheric O_3 mixing ratio, we have conducted simulations without (experiment: noLNOx) and with (experiment: wLNOx) LNOx emissions. After comparing the results from these experiments, an increase of 2–5 ppbv in the annual mean of O_3 mixing ratio at the surface, is observed due to the inclusion of LNOx, over most of the NH region. The increase is 2–3 times larger over the tropical lands, where a high lightning flash rate is found. The change in simulated NO_2 at the surface is negligible in comparison and exhibits a moderately acceptable agreement with the ground-based observations at available stations. The simulated O_3 at surface is however in good agreement with observations, showing comparatively lower absolute mean bias and errors. There is an overall increase in O_3 observed in the troposphere due to the inclusion of LNOx and shows a maximum increase in the mid to upper troposphere, specifically over the tropics, where extreme lightning discharge occurs. We successfully simulate the mid to upper tropospheric O_3 over the tropical region in experiment wLNOx, reducing the absolute bias in simulated O_3 in comparison to ozone sonde measurements. The tropospheric O_3 burden over NH is increased from 116.53 Tg to 133.63 Tg due to the inclusion of LNOx. The high underestimation in simulated O_3, at free troposphere over mid-latitudes and polar regions, indicates inadequate vertical mixing and representation of convection and stratosphere-troposphere exchange.

In our study, we also have shown the impact of LNOx on hydroxyl radical (OH) burden and lifetime of trace gas methane (CH_4). The average tropospheric OH concentration is estimated as 14×10^5 molecules cm^{-3} over NH, which is highest over the tropics, especially in the mid-troposphere. The tropospheric OH concentration is slightly higher than that estimated from previous model-based studies and the CH_4 lifetime is reduced to a comparatively lower value of 4.89 years. Here, we estimate the CH_4 lifetime due to chemical loss through the reaction with OH radical. Hence, in the presence of LNOx, the OH burden increases by 40% and the average lifetime of CH_4 reduces by 24% over the NH. Our study further suggests investigating the effects of initial chemical boundary conditions and the source–sink pathways of OH in the CHIMERE model for further improvement in OH burden and CH_4 lifetime estimation.

https://doi.org/10.5194/egusphere-2024-3087
Preprint. Discussion started: 5 November 2024

Code and data availability. The CHIMERE model (v2023r2) is available on the website at https://www.lmd.polytechnique.fr/chimere/. The measurement data used in the study are all freely downloadable from cited URLs.

Author contributions. SG analysed the model output and data, downloaded satellite data, made plots, conceptualised and prepared a first version of the manuscript. AC performed the simulations and contributed to the measurement data collection. All co-authors have participated in the conception of the study, the interpretation and discussion of the results, and the redaction of the final manuscript.

Competing interests. The authors declare that they have no conflict of interest.

Acknowledgements. This study was supported by the Agence de l'Environnement et de la Maîtrise de l'Energie (ADEME) within the framework of the ESCALAIR project (grant: 2162D0017). We also acknowledge the use of computational resources provided by the GENCI GEN10274 project.

https://doi.org/10.5194/egusphere-2024-3087
Preprint. Discussion started: 5 November 2024

References

Akimoto, H. and Tanimoto, H.: Rethinking of the adverse effects of NOx-control on the reduction of methane and tropospheric ozone–challenges toward a denitrified society, Atmospheric Environment, 277, 119 033, https://doi.org/10.1016/j.atmosenv.2022.119033, 2022.

Alfaro, S. C. and Gomes, L.: Modeling mineral aerosol production by wind erosion: Emission intensities and aerosol size distributions in source areas, Journal of Geophysical Research: Atmospheres, 106, 18 075–1808, https://doi.org/10.1029/2000JD900339, 2001.

Allen, D., Pickering, K., Stenchikov, G., Thompson, A., and Kondo, Y.: A three-dimensional total odd nitrogen (NOy) simulation during SONEX using a stretched-grid chemical transport model, Journal of Geophysical Research: Atmospheres, 105, 3851–3876, https://doi.org/10.1029/1999JD901029, 2000.

Allen, D., Pickering, K., Duncan, B., and Damon, M.: Impact of lightning NO emissions on North American photochemistry as determined using the Global Modeling Initiative (GMI) model, Journal of Geophysical Research: Atmospheres, 115, 2010.

Allen, D. J. and Pickering, K. E.: Evaluation of lightning flash rate parameterizations for use in a global chemical transport model, Journal of Geophysical Research: Atmospheres, 107, ACH–15, https://doi.org/10.1029/2002JD002066, 2002.

Allen, D. J., Pickering, K. E., Pinder, R. W., Henderson, B. H., Appel, K. W., and Prados, A.: Impact of lightning-NO on eastern United States photochemistry during the summer of 2006 as determined using the CMAQ model, Atmospheric Chemistry and Physics, 12, 1737–1758, https://doi.org/10.5194/acp-12-1737-2012, 2012.

Arndt, J. A., Aulinger, A., and Matthias, V.: Quantification of lightning-induced nitrogen oxide emissions over Europe, Atmospheric Environment, 202, 128–141, 2019.

Banerjee, A., Archibald, A. T., Maycock, A. C., Telford, P., Abraham, N. L., Yang, X., Braesicke, P., and Pyle, J. A.: Lightning NOx, a key chemistry–climate interaction: impacts of future climate change and consequences for tropospheric oxidising capacity, Atmospheric Chemistry and Physics, 14, 9871–9881, 2014.

Bessagnet, B., Menut, L., Curci, G., Hodzic, A., Guillaume, B., Liousse, C., Moukhtar, S., Pun, B., Seigneur, C., and Schulz, M.: Regional modeling of carbonaceous aerosols over Europe–focus on secondary organic aerosols, Journal of Atmospheric Chemistry, 61, 175–202, https://doi.org/10.1007/s10874-009-9129-2, 2008.

Blakeslee, R. J., Lang, T. J., Koshak, W. J., Buechler, D., Gatlin, P., Mach, D. M., Stano, G. T., Virts, K. S., Walker, T. D., Cecil, D. J., Ellett, W., Goodman, S. J., Harrison, S., Hawkins, D. L., Heumesser, M., Lin, H., Maskey, M., Schultz, C. J., Stewart, M., Bateman, M., Chanrion, O., and Christian, H.: Three Years of the Lightning Imaging Sensor Onboard the International Space Station: Expanded Global Coverage and Enhanced Applications, Journal of Geophysical Research: Atmospheres, 125, e2020JD032 918, https://doi.org/10.1029/2020JD032918, 2020.

Boccippio, D. J.: Lightning Scaling Relations Revisited, Journal of the Atmospheric Sciences, 59, 1086–1104, https://doi.org/10.1175/1520-0469(2002)059<1086:LSRR>2.0.CO;2, 2002.

Burkholder, J. B., Sander, S. P., Abbatt, J., Barker, J. R., Cappa, C., Crounse, J. D., Dibble, T. S., Huie, R. E., Kolb, C. E., Kurylo, M. J., Orkin, V. L., Percival, C. J., Wilmouth, D. M., and Wine, P. H.: Chemical Kinetics and Photochemical Data for Use in Atmospheric Studies, Evaluation No. 19, Jet Propulsion Laboratory, Pasadena, http://jpldataeval.jpl.nasa.gov, 2019.

Butler, T., Lupascu, A., and Nalam, A.: Attribution of ground-level ozone to anthropogenic and natural sources of nitrogen oxides and reactive carbon in a global chemical transport model, Atmospheric Chemistry and Physics, 20, 10 707–10 731, https://doi.org/10.5194/acp-20-10707-2020, 2020.

https://doi.org/10.5194/egusphere-2024-3087
Preprint. Discussion started: 5 November 2024

Cheng, P., Pour-Biazar, A., Wu, Y., Kuang, S., McNider, R. T., and Koshak, W. J.: Utility of Geostationary Lightning Mapper-derived lightning NO emission estimates in air quality modeling studies, Atmospheric Chemistry and Physics, 24, 41–63, https://doi.org/10.5194/acp-24-41-2024, 2024.

Chin, M., Ginoux, P., Kinne, S., Torres, O., Holben, B. N., Duncan, B. N., Martin, R. V., Logan, J. A., Higurashi, A., and Nakajima, T.: Tropospheric Aerosol Optical Thickness from the GOCART Model and Comparisons with Satellite and Sun Photometer Measurements, Journal of the Atmospheric Sciences, 59, 461–483, https://doi.org/10.1175/1520-0469(2002)059<0461:TAOTFT>2.0.CO;2, 2002.

Choi, Y., Wang, Y., Zeng, T., Martin, R. V., Kurosu, T. P., and Chance, K.: Evidence of lightning NOx and convective transport of pollutants in satellite observations over North America, Geophysical Research Letters, 32, https://doi.org/10.1029/2004GL021436, 2005.

Christian, H. J. and Petersen, W.: Global lightning activity, in: Conference on Meteorological Applications of Lightning Data, 85th AMS Annual Meeting, San Diego, CA, pp. 10–12, 2005.

Clark, S. K., Ward, D. S., and Mahowald, N. M.: Parameterization-based uncertainty in future lightning flash density, Geophysical Research Letters, 44, 2893–2901, https://doi.org/10.1002/2017GL073017, 2017.

Després, B. and Lagoutière, F.: A non-linear anti-diffusive scheme for the linear advection equation, Comptes Rendus de l'Académie des Sciences-Series I-Mathematics, 328, 939–943, https://doi.org/10.1016/S0764-4442(99)80301-2, 1999.

Dufour, G., Hauglustaine, D., Zhang, Y., Eremenko, M., Cohen, Y., Gaudel, A., Siour, G., Lachatre, M., Bense, A., Bessagnet, B., et al.: Recent ozone trends in the Chinese free troposphere: role of the local emission reductions and meteorology, Atmospheric Chemistry and Physics, 21, 16 001–16 025, https://doi.org/10.5194/acp-21-16001-2021, 2021.

Erdmann, F., Defer, E., Caumont, O., Blakeslee, R. J., Pédeboy, S., and Coquillat, S.: Concurrent satellite and ground-based lightning observations from the Optical Lightning Imaging Sensor (ISS-LIS), the low-frequency network Meteorage and the SAETTA Lightning Mapping Array (LMA) in the northwestern Mediterranean region, Atmospheric Measurement Techniques, 13, 853–875, https://doi.org/10.5194/amt-13-853-2020, 2020.

Finney, D., Doherty, R., Wild, O., and Abraham, N. L.: The impact of lightning on tropospheric ozone chemistry using a new global lightning parametrisation, Atmospheric Chemistry and Physics, 16, 7507–7522, https://doi.org/10.5194/acp-16-7507-2016, 2016a.

Finney, D. L., Doherty, R. M., Wild, O., Huntrieser, H., Pumphrey, H. C., and Blyth, A. M.: Using cloud ice flux to parametrise large-scale lightning, Atmospheric Chemistry and Physics, 14, 12 665–12 682, https://doi.org/10.5194/acp-14-12665-2014, 2014.

Finney, D. L., Doherty, R. M., Wild, O., Young, P. J., and Butler, A.: Response of lightning NOx emissions and ozone production to climate change: Insights from the Atmospheric Chemistry and Climate Model Intercomparison Project, Geophysical Research Letters, 43, 5492–5500, https://doi.org/10.1002/2016GL068825, 2016b.

Ghosh, A., Patra, P. K., Ishijima, K., Umezawa, T., Ito, A., Etheridge, D. M., Sugawara, S., Kawamura, K., Miller, J. B., Dlugokencky, E. J., Krummel, P. B., Fraser, P. J., Steele, L. P., Langenfelds, R. L., Trudinger, C. M., White, J. W. C., Vaughn, B., Saeki, T., Aoki, S., and Nakazawa, T.: Variations in global methane sources and sinks during 1910–2010, Atmospheric Chemistry and Physics, 15, 2595–2612, https://doi.org/10.5194/acp-15-2595-2015, 2015.

Gordillo-Vázquez, F. J., Pérez-Invernón, F. J., Huntrieser, H., and Smith, A. K.: Comparison of Six Lightning Parameterizations in CAM5 and the Impact on Global Atmospheric Chemistry, Earth and Space Science, 6, 2317–2346, https://doi.org/10.1029/2019EA000873, 2019.

Guenther, A. B., Jiang, X., Heald, C. L., Sakulyanontvittaya, T., Duhl, T., Emmons, L. K., and Wang, X.: The Model of Emissions of Gases and Aerosols from Nature version 2.1 (MEGAN2.1): an extended and updated framework for modeling biogenic emissions, Geoscientific Model Development, 5, 1471–1492, https://doi.org/10.5194/gmd-5-1471-2012, 2012.

https://doi.org/10.5194/egusphere-2024-3087
Preprint. Discussion started: 5 November 2024

Hasenkopf, C. A., Flasher, J. C., Veerman, O., and DeWitt, H. L.: OpenAQ: a platform to aggregate and freely share global air quality data, in: AGU Fall Meeting Abstracts, vol. 2015, pp. A31D–0097, 2015.

Hauglustaine, D. A., Balkanski, Y., and Schulz, M.: A global model simulation of present and future nitrate aerosols and their direct radiative forcing of climate, Atmospheric Chemistry and Physics, 14, 11 031–11 063, https://doi.org/10.5194/acp-14-11031-2014, 2014.

Kang, D., Foley, K. M., Mathur, R., Roselle, S. J., Pickering, K. E., and Allen, D. J.: Simulating lightning NO production in CMAQv5. 2: performance evaluations, Geoscientific model development, 12, 4409–4424, https://doi.org/10.5194/gmd-12-4409-2019, 2019.

Kang, D., Mathur, R., Pouliot, G. A., Gilliam, R. C., and Wong, D. C.: Significant ground-level ozone attributed to lightning-induced nitrogen oxides during summertime over the Mountain West States, NPJ climate and atmospheric science, 3, 6, https://doi.org/10.1038/s41612-020-0108-2, 2020.

Labrador, L. J., von Kuhlmann, R., and Lawrence, M. G.: The effects of lightning-produced NOx and its vertical distribution on atmospheric chemistry: sensitivity simulations with MATCH-MPIC, Atmospheric Chemistry and Physics, 5, 1815–1834, https://doi.org/10.5194/acp-5-1815-2005, 2005.

Lachatre, M., Mailler, S., Menut, L., Turquety, S., Sellitto, P., Guermazi, H., Salerno, G., Caltabiano, T., and Carboni, E.: New strategies for vertical transport in chemistry transport models: application to the case of the Mount Etna eruption on 18 March 2012 with CHIMERE v2017r4, Geoscientific Model Development, 13, 5707–5723, https://doi.org/10.5194/gmd-13-5707-2020, 2020.

Lelieveld, J. and Dentener, F. J.: What controls tropospheric ozone?, Journal of Geophysical Research: Atmospheres, 105, 3531–3551, https://doi.org/10.1029/1999JD901011, 2000.

Lelieveld, J., Gromov, S., Pozzer, A., and Taraborrelli, D.: Global tropospheric hydroxyl distribution, budget and reactivity, Atmospheric Chemistry and Physics, 16, 12 477–12 493, https://doi.org/10.5194/acp-16-12477-2016, 2016.

Li, M., Mao, J., Chen, S., Bian, J., Bai, Z., Wang, X., Chen, W., and Yu, P.: Significant contribution of lightning NOx to summertime surface O3 on the Tibetan Plateau, Science of The Total Environment, 829, 154 639, https://doi.org/10.1016/j.scitotenv.2022.154639, 2022.

Luhar, A. K., Galbally, I. E., Woodhouse, M. T., and Abraham, N. L.: Assessing and improving cloud-height-based parameterisations of global lightning flash rate, and their impact on lightning-produced NO x and tropospheric composition in a chemistry–climate model, Atmospheric Chemistry and Physics, 21, 7053–7082, https://doi.org/10.5194/acp-21-7053-2021, 2021.

Luhar, A. K., Jones, A. C., and Wilkinson, J. M.: Quantifying the impact of global nitrate aerosol on tropospheric composition fields and its production from lightning NO_x, EGUsphere, 2024, 1–38, https://doi.org/10.5194/egusphere-2024-1363, 2024.

Luo, C., Wang, Y., and Koshak, W. J.: Development of a self-consistent lightning NOx simulation in large-scale 3-D models, Journal of Geophysical Research: Atmospheres, 122, 3141–3154, https://doi.org/10.1002/2016JD026225, 2017.

Mailler, S., Menut, L., di Sarra, A. G., Becagli, S., Di Iorio, T., Bessagnet, B., Briant, R., Formenti, P., Doussin, J.-F., Gómez-Amo, J. L., Mallet, M., Rea, G., Siour, G., Sferlazzo, D. M., Traversi, R., Udisti, R., and Turquety, S.: On the radiative impact of aerosols on photolysis rates: comparison of simulations and observations in the Lampedusa island during the ChArMEx/ADRIMED campaign, Atmospheric Chemistry and Physics, 16, 1219–1244, https://doi.org/10.5194/acp-16-1219-2016, 2016.

Maseko, B., Feig, G., and Burger, R.: Estimating lightning NOx production over South Africa, South African Journal of Science, 117, 1–11, https://doi.org/10.17159/sajs.2021/8035, 2021.

Menut, L., Bessagnet, B., Khvorostyanov, D., Beekmann, M., Blond, N., Colette, A., Coll, I., Curci, G., Foret, G., Hodzic, A., Mailler, S., Meleux, F., Monge, J. L., Pison, I., Siour, G., Turquety, S., Valari, M., Vautard, R., and Vivanco, M. G.: CHIMERE 2013: a model for regional atmospheric composition modelling, Geoscientific Model Development, 6, 981–1028, https://doi.org/10.5194/gmd-6-981-2013, 2013.

https://doi.org/10.5194/egusphere-2024-3087
Preprint. Discussion started: 5 November 2024

Menut, L., Bessagnet, B., Mailler, S., Pennel, R., and Siour, G.: Impact of lightning NOx emissions on atmospheric composition and meteorology in Africa and Europe, Atmosphere, 11, 1128, https://doi.org/10.3390/atmos11101128, 2020a.

Menut, L., Bessagnet, B., Siour, G., Mailler, S., Pennel, R., and Cholakian, A.: Impact of lockdown measures to combat Covid-19 on air quality over western Europe, Science of The Total Environment, 741, 140 426, https://doi.org/10.1016/j.scitotenv.2020.140426, 2020b.

Menut, L., Bessagnet, B., Briant, R., Cholakian, A., Couvidat, F., Mailler, S., Pennel, R., Siour, G., Tuccella, P., Turquety, S., and Valari, M.: The CHIMERE v2020r1 online chemistry-transport model, Geoscientific Model Development, 14, 6781–6811, https://doi.org/10.5194/gmd-14-6781-2021, 2021.

Menut, L., Cholakian, A., Pennel, R., Siour, G., Mailler, S., Valari, M., Lugon, L., and Meurdesoif, Y.: The CHIMERE chemistry-transport model v2023r1, Geoscientific Model Development Discussions, 2024, 1–44, https://doi.org/10.5194/gmd-17-5431-2024, 2024.

Michalon, N., Nassif, A., Saouri, T., Royer, J. F., and Pontikis, C. A.: Contribution to the climatological study of lightning, Geophysical Research Letters, 26, 3097–3100, https://doi.org/10.1029/1999GL010837, 1999.

Monahan, E. C.: The Ocean as a Source for Atmospheric Particles, pp. 129–163, Springer Netherlands, https://doi.org/10.1007/978-94-009-4738-2_6, 1986.

Murray, L. T.: Lightning NOx and impacts on air quality, Current Pollution Reports, 2, 115–133, 2016.

Murray, L. T., Jacob, D. J., Logan, J. A., Hudman, R. C., and Koshak, W. J.: Optimized regional and interannual variability of lightning in a global chemical transport model constrained by LIS/OTD satellite data, Journal of Geophysical Research: Atmospheres, 117, 2012.

Murray, L. T., Logan, J. A., and Jacob, D. J.: Interannual variability in tropical tropospheric ozone and OH: The role of lightning, Journal of Geophysical Research: Atmospheres, 118, 11–468, 2013.

Murray, L. T., Fiore, A. M., Shindell, D. T., Naik, V., and Horowitz, L. W.: Large uncertainties in global hydroxyl projections tied to fate of reactive nitrogen and carbon, Proceedings of the National Academy of Sciences, 118, e2115204 118, https://doi.org/10.1073/pnas.2115204118, 2021.

Naik, V., Voulgarakis, A., Fiore, A. M., Horowitz, L. W., Lamarque, J.-F., Lin, M., Prather, M. J., Young, P. J., Bergmann, D., Cameron-Smith, P. J., Cionni, I., Collins, W. J., Dalsøren, S. B., Doherty, R., Eyring, V., Faluvegi, G., Folberth, G. A., Josse, B., Lee, Y. H., MacKenzie, I. A., Nagashima, T., van Noije, T. P. C., Plummer, D. A., Righi, M., Rumbold, S. T., Skeie, R., Shindell, D. T., Stevenson, D. S., Strode, S., Sudo, K., Szopa, S., and Zeng, G.: Preindustrial to present-day changes in tropospheric hydroxyl radical and methane lifetime from the Atmospheric Chemistry and Climate Model Intercomparison Project (ACCMIP), Atmospheric Chemistry and Physics, 13, 5277–5298, https://doi.org/10.5194/acp-13-5277-2013, 2013.

Nault, B. A., Laughner, J. L., Wooldridge, P. J., Crounse, J. D., Dibb, J., Diskin, G., Peischl, J., Podolske, J. R., Pollack, I. B., Ryerson, T. B., Scheuer, E., Wennberg, P. O., and Cohen, R. C.: Lightning NOx Emissions: Reconciling Measured and Modeled Estimates With Updated NO Chemistry, Geophysical Research Letters, 44, 9479–9488, https://doi.org/10.1002/2017GL074436, 2017.

Pawar, S. D., Lal, D. M., and Murugavel, P.: Lightning characteristics over central India during Indian summer monsoon, Atmospheric Research, 106, 44–49, https://doi.org/10.1016/j.atmosres.2011.11.007, 2012a.

Pawar, V., Pawar, S. D., Beig, G., and Sahu, S. K.: Effect of lightning activity on surface NOx and O_3 over a tropical station during pre-monsoon and monsoon seasons, Journal of Geophysical Research: Atmospheres, 117, D05 310, https://doi.org/10.1029/2011JD016930, 2012b.

Price, C. and Rind, D.: A simple lightning parameterization for calculating global lightning distributions, Journal of Geophysical Research: Atmospheres, 97, 9919–9933, https://doi.org/10.1029/92JD00719, 1992.

https://doi.org/10.5194/egusphere-2024-3087
Preprint. Discussion started: 5 November 2024

Price, C. and Rind, D.: What determines the cloud-to-ground lightning fraction in thunderstorms?, Geophysical Research Letters, 20, 463–466, https://doi.org/10.1029/93GL00226, 1993.

Price, C., Penner, J., and Prather, M.: NOx from lightning: 1. Global distribution based on lightning physics, Journal of Geophysical Research: Atmospheres, 102, 5929–5941, https://doi.org/10.1029/96JD03504., 1997a.

Price, C., Penner, J., and Prather, M.: NOx from lightning: 2. Constraints from the global atmospheric electric circuit, Journal of Geophysical Research: Atmospheres, 102, 5943–5951, https://doi.org/10.1029/96JD02551, 1997b.

Price, C., Penner, J., and Prather, M.: NOx from lightning: 2. Constraints from the global atmospheric electric circuit, Journal of Geophysical Research: Atmospheres, 102, 5943–5951, https://doi.org/10.1029/96JD02551, 1997c.

Pun, B. K. and Seigneur, C.: Investigative modeling of new pathways for secondary organic aerosol formation, Atmospheric Chemistry and Physics, 7, 2199–2216, https://doi.org/10.5194/acp-7-2199-2007, 2007.

Schumann, U. and Huntrieser, H.: The global lightning-induced nitrogen oxides source, Atmospheric Chemistry and Physics, 7, 3823–3907, https://doi.org/10.5194/acp-7-3823-2007, 2007.

Tiedtke, M.: A comprehensive mass flux scheme for cumulus parameterization in large-scale models, Monthly Weather Reviews, 117, 1779–1800, https://doi.org/10.1175/1520-0493(1989)117<1779:ACMFSF>2.0.CO;2, 1989.

Troen, I. and Mahrt, L.: A simple model of the atmospheric boundary layer: Sensitivity to surface evaporation, Boundary-Layer Meteorology, 37, 129–148, https://doi.org/10.1007/BF00122760, 1986.

van der A, R. J., Eskes, H. J., Boersma, K. F., van Noije, T. P. C., Van Roozendael, M., De Smedt, I., Peters, D. H. M. U., and Meijer, E. W.: Trends, seasonal variability and dominant NOx source derived from a ten year record of NO2 measured from space, Journal of Geophysical Research: Atmospheres, 113, D04 302, https://doi.org/10.1029/2007JD009021, 2008.

van Leer, B.: Towards the ultimate conservative difference scheme: IV. A new approach to numerical convection, Journal of Computational Physics, 23, 276–299, https://doi.org/10.1016/0021-9991(77)90095-X, 1977.

Verma, S., Yadava, P. K., Lal, D. M., Mall, R. K., Kumar, H., and Payra, S.: Role of Lightning NOx in Ozone Formation: A Review, Pure and Applied Geophysics, 178, 1425–1443, https://doi.org/10.1007/s00024-021-02710-5, 2021.

von Kuhlmann, R., Lawrence, M. G., Crutzen, P. J., and Rasch, P. J.: A model for studies of tropospheric ozone and nonmethane hydrocarbons: Model description and ozone results, Journal of Geophysical Research: Atmospheres, 108, https://doi.org/10.1029/2002JD002893, 2003.

Vonnegut, B.: Some facts and speculations concerning the origin and role of thunderstorm electricity, pp. 224–241, American Meteorological Society, https://doi.org/10.1007/978-1-940033-56-3_11, 1963.

Voulgarakis, A., Naik, V., Lamarque, J.-F., Shindell, D. T., Young, P. J., Prather, M. J., Wild, O., Field, R. D., Bergmann, D., Cameron-Smith, P., Cionni, I., Collins, W. J., Dalsøren, S. B., Doherty, R. M., Eyring, V., Faluvegi, G., Folberth, G. A., Horowitz, L. W., Josse, B., MacKenzie, I. A., Nagashima, T., Plummer, D. A., Righi, M., Rumbold, S. T., Stevenson, D. S., Strode, S. A., Sudo, K., Szopa, S., and Zeng, G.: Analysis of present day and future OH and methane lifetime in the ACCMIP simulations, Atmospheric Chemistry and Physics, 13, 2563–2587, https://doi.org/10.5194/acp-13-2563-2013, 2013.

Wesely, M.: Parameterization of Surface Resistances to Gaseous Dry Deposition in Regional-Scale Numerical Models, Atmospheric Environment, 23, 1293–1304, https://doi.org/10.1016/0004-6981(89)90153-4, 1989.

Wild, O., Zhu, X., and Prather, M. J.: Fast-J: Accurate Simulation of In- and Below-Cloud Photolysis in Tropospheric Chemical Models, Journal of Atmospheric Chemistry, 37, 245–282, https://doi.org/10.1023/A:1006415919030, 2000.

https://doi.org/10.5194/egusphere-2024-3087
Preprint. Discussion started: 5 November 2024

Williams, E. R.: Large-scale charge separation in thunderclouds, Journal of Geophysical Research: Atmospheres, 90, 6013–6025, https://doi.org/10.1029/JD090iD04p06013, 1985.

Wu, Y., Pour-Biazar, A., Koshak, W., and Cheng, P.: LNOx emission model for air quality and climate studies using satellite lightning mapper observations, Journal of Geophysical Research: Atmospheres, 128, e2022JD037 406, https://doi.org/10.1029/2022JD037406, 2023.

Xu, M., Qie, X., Zhao, C., Yuan, S., Li, J., Tao, Y., Shi, G., Pang, W., and Shi, L.: Distribution of lightning spatial modes and climatic causes in China, Atmospheric and Oceanic Science Letters, 16, 100 338, https://doi.org/10.1016/j.aosl.2023.100338, 2023.

Young, P. J., Archibald, A. T., Bowman, K. W., Lamarque, J.-F., Naik, V., Stevenson, D. S., Tilmes, S., Voulgarakis, A., Wild, O., Bergmann, D., Cameron-Smith, P., Cionni, I., Collins, W. J., Dalsøren, S. B., Doherty, R. M., Eyring, V., Faluvegi, G., Horowitz, L. W., Josse, B., Lee, Y. H., MacKenzie, I. A., Nagashima, T., Plummer, D. A., Righi, M., Rumbold, S. T., Skeie, R. B., Shindell, D. T., Strode, S. A., Sudo, K., Szopa, S., and Zeng, G.: Pre-industrial to end 21st century projections of tropospheric ozone from the Atmospheric Chemistry and Climate Model Intercomparison Project (ACCMIP), Atmospheric Chemistry and Physics, 13, 2063–2090, https://doi.org/10.5194/acp-13-2063-2013, 2013.

Zhang, D., Cummins, K. L., Lang, T. J., Buechler, D., and Rudlosky, S.: Performance Evaluation of the Lightning Imaging Sensor on the International Space Station, Journal of Atmospheric and Oceanic Technology, 40, 1063–1082, https://doi.org/10.1175/JTECH-D-22-0120.1, 2023.

Zhang, L., Gong, S., Padro, J., and Barrie, L.: A size-segregated particle dry deposition scheme for an atmospheric aerosol module, Atmospheric Environment, 35(3), 549–560, https://doi.org/10.1016/S1352-2310(00)00326-5, 2001.

Zhao, C., Wang, Y., Choi, Y., and Zeng, T.: Summertime impact of convective transport and lightning NOx production over North America: modeling dependence on meteorological simulations, Atmospheric Chemistry and Physics, 9, 4315–4327, https://doi.org/www.atmos-chem-phys.net/9/4315/2009/, 2009.

Zhao, Y., Saunois, M., Bousquet, P., Lin, X., Hegglin, M. I., Canadell, J. G., Jackson, R. B., and Zheng, B.: Reconciling the bottom-up and top-down estimates of the methane chemical sink using multiple observations, Atmospheric Chemistry and Physics, 23, 789–807, https://doi.org/10.5194/acp-23-789-2023, 2023.